united nations educational, scientific and cultural organization

international atomic energy agency

the
abdus salam
international centre for theoretical physics

H4.SMR/1304-27

"COLLEGE ON SOIL PHYSICS"

12 March - 6 April 2001

WATER EROSION PROCESSES AND MODELLING

Donald GABRIELS

University of Ghent
Laboratory of Soil Physics
Dept. Soil Management & Soil Care
Faculty of Agriculture & Spplied Biological Sciences
Ghent, Belgium

<u>These notes are for internal distribution only</u>

THE UNIVERSIAL SOIL LOSS EQUATION (USLE) FOR PREDICTING RAINFALL EROSION LOSSES

D. GABRIELS

National Fund for Scientific Research
Laboratory for Soil Physics
Rijksuniversiteit Gent
Coupure Links 653
B-9000 Gent, Belgium

ABSTRACT

Soil loss equations have been developed to understand the erosion process and to predict field soil losses. The equation most widely used today for soil loss prediction from sheet-interrill-rill erosion is the Universal Soil Loss Equation (USLE). It computes the soil loss for a given site as the product of six major factors, each given a numerical value. These factors are the rainfall erosivity (R), the soil erodibility (K), the slope length factor (L), the slope steepness factor (S) and the erosion control practice (P).

1. INTRODUCTION

Soil erosion has been described as the removal of inorganic as well as organic soil surface material by wind and water. Grazing, land clearing, plant harvesting without proper soil management rapidly deplete and exhaust the soil of organic matter and nutrients. This process is important everywhere, although most dramatic in arid and semi-arid regions where marginal lands are rapidly converted into deserts.

Water erosion takes place under the action of water as rainfall and runoff by detaching and transporting soil particles. The most important causes of water erosion are therefore the characteristics of rainfall, soil and land.

Most of the knowledge of soil erosion mechanisms and rates originates in the work of the U.S. Soil Conservation Service with the development of the Universal Soil Loss Equation (USLE), an estimation of erosion as the product of a series of terms for rainfall, slope gradient, slope length, soil, and cropping factors.

This equation is now a widely used model for predicting sheet and rill erosion (Wischmeier and Smith, 1978). It has the form:

$$A = R \times K \times L \times S \times C \times P$$

with the soil loss (A), the rainfall erosivity (R), the soil erodibility (K), the cropping-management factor (C), the erosion control practice factor (P), and the topographic factors: the slope length factor (L) and slope steepness factor (S).

The factors of the USLE were developed using a standard plot which is 22.13 m long on a 9% slope. The plot was tilled up and down slope and was in continuous fallow for at least two years. The standard plot is a result of the historical development of the USLE when early basic data were obtained from 0.01 acre plots (40.5 m^2). For a 6 ft width (1.83 m), this gave a plot length of 22.13 m (72.6 ft).

2. THE RAINFALL EROSIVITY FACTOR R

Rainfall erosivity is defined as the potential ability of rain to cause erosion or the agressivity of rainfall to induce erosion. In the USLE, the factor R is defined as a rainfall and runoff factor and the product of two rainstorm characteristics: kinetic energy and the maximum 30 minute intensity.

In quantifying rainfall erosivity the size, distribution and terminal velocity of individual raindrops need to be characterized. Many studies have been made of raindrop size (Laws and Parsons, 1943; Mihara, 1952; Hudson, 1964). It was found that the upper limit of the size appears to be about 5-6 mm in diameter. Studies, such as those of Best (1950) and Hudson (1963) showed the size distribution of the raindrops depending on the rainintensity, with an increasing drop size with increasing intensity for low intensities.But at very high intensities (higher than 100 mm/hr) a reversal of the trend is observed (Hudson, 1963). Carter et al. (1974) on the other hand showed that at intensities over 250 mm/hr the greatest proportion of raindrops is larger than 4 mm in diameter. Probably, at intensities higher than 200 mm per hour, coallescence of smaller drops again take place (Evans, 1980).

Laws (1941) measured the velocity of waterdrops falling from different heights. These measurements, using high speed photography, resulted in a relationship between terminal velocity and diameter of raindrops as shown in figure 1. Gunn and Kinzer (1949) confirmed these results.

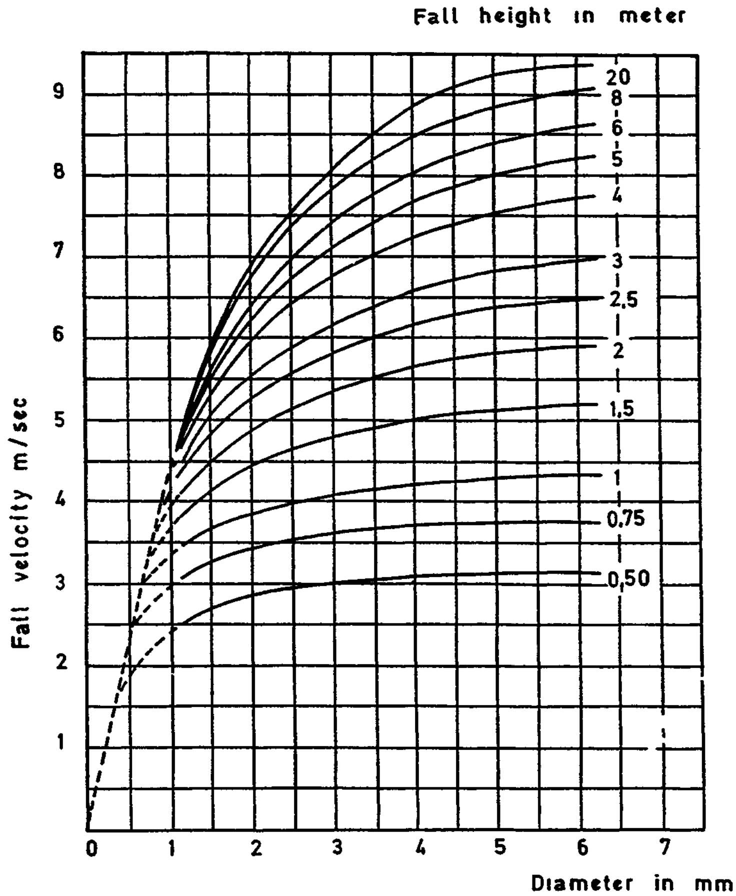

Figure 1 : Relationship between dropdiameter and fall velocity for different fall heights (after Laws, 1941)

Ellison (1944) and Bisal (1960) showed that soil detachment and/or splash erosion are related to the mass and velocity of falling drops. Mihara (1959) and Free (1960) found that splash erosion is directly correlated with kinetic energy. Kinetic energy of a falling raindrop may be computed indirectly when the drop size and the terminal velocity are known. Kinetic energy may also be determined by converting the kinetic energy into another form of energy which may be more easily measured, such as with an acoustic recorder (Kinnell, 1968; Forrest, 1970; De Wulf and Gabriels, 1982). But studies on this line are still continuing.

Different authors found different relationships between kinetic energy (E) and intensity (I) of rainfall:

Mihara (1952): $E = 75.9I^{1.2}$

with E: $erg/cm^2.minute$

I: $mg/cm^2.minute$

Wischmeier and Smith (1958):

$E = 916 + 331 \log I$

with E: foot ton/acre.inch

I: inch/hour

in metric units the expression is:

$E = 1.213 + 0.890 \log_{10} I$

with E: kg m/m^2 mm

I: mm/hour

In Zimbabwe, Hudson (1965) found:

$$E = 758.52 - \frac{127.51}{I}$$

with E: ergs x $10^3/cm^2$

I: inch/hour

For the Miami area, Kinnell (1973) found:

$E = 8.37\ I - 45.9$

with E: $ergs/cm^2$ sec

I: mm/hr

Carter et al. (1974) found in Louisiana and Mississippi:

$$E = 429.2 + 534.0\ I - 122.5\ I^2 + 78\ I^3$$

with E: foot ton/acre.inch

I: inch/hour

It is clear that there is a good correlation between kinetic energy and rainfall intensity, but the equation and regression coefficient expressing the relationship are different from one place to another, depending on the climatic condition.

Wischmeier and Smith (1958) found as a result of extensive statistical analysis that EI_{30}, the product of the total energy of a rainstorm (E) and the storm's maximum intensity for a 30-minute duration (I_{30}) gave the best correlation with soil loss.

The EI_{30} index has been widely used in America, and other countries such as: India (Bhatia and Singh, 1976), West and Central Africa (Roose, 1977), Indonesia (Bols, 1978), Belgium (Bollinne et al., 1980). However, the index has not been entirely satisfactory, particularly for the tropical rainstorms (Lal, 1976). This author indicated that EI_{30} may underestimate the kinetic energy of tropical storms. Hudson and Jackson (1959) found in Rhodesia that the EI_{30} index was not efficient as might be expected from Wischmeier's studies in U.S. Ahmad and Breckner (1974) found in Trinidad that the correlations of this index with soil loss were generally low.

Hudson (1971) proposed an alternative method for estimating the erosivity of rainfall. He defined the KE > 1 index as the sum of the kinetic energies in storms with intensities greater than 1 in/hr (25 mm/hr). It is based on the concept that there is a threshold value of intensity at which rain starts to become erosive. Such an index could be more adequate for describing rainfall erosion hazards for tropical soils, which are generally characterized by well-structured profiles and infiltration rates greater than 1 in/hr.

Lal (1976) proposed the AI_m index being the product of total rainfall (A) in cm and maximum intensity (Im) in cm/hour for a minimum duration of 7.5 minutes.

Fournier (1960) in his attempt to correlate climatic parameters to suspended sediment load in rivers defined a rainfall distribution coefficient C as p_m^2/P where p_m is the mean rainfall for the wettest month of the year and P the mean annual rainfall. Soil erosion can be estimated using this coefficient only insofar as the suspended sediment load of a river is related to the soil loss for the whole catchment. Arnoldus (1980) obtained poor correlations between the EI_{30} and Fournier's indices. He proposed the modification:

$$\sum_{1}^{12} p_i^{\,2}/P$$

in which p_i is the monthly precipitation and P is the annual precipitation.

3. THE SOIL ERODIBILITY FACTOR K

The soil erodibility factor K in the universal soil loss equation describes the susceptibility of the soil to erosion and reflects the fact that different soils erode at different rates when the other factors that affect erosion are the same. As intended by the USLE, the experimental determination of K must be based on unit values for other factors in the equation (see further).

The inherent susceptibility of a soil to erosion by water is collectively determined by its structural and hydrological properties. Aggregate breakdown and particle detachment depend on aggregate stability and particle size distribution characterisitcs. The particle-transporting runoff depends not only on rainfall characteristics but also on water transmission and rillability properties of the soil, particularly infiltration rates at the prevailing antecedent water contents.

The dependence of soil susceptibility to water erosion on textural, structural, and hydrological properties has been established by several investigators (Wischmeier and Mannering, 1969; Wischmeier et al., 1971; Roth et al., 1974). They developed equations and nomographs which were recommended for estimating K-values whenever experimental values are not available (figure 2 and figure 3). These nomographs were widely used in the U.S. and in many other countries, including tropical. El-Swaify (1977) and El-Swaify and Dangler (1977) however criticized the use of the nomographs to predict the erodibility of tropical soils.

4. THE TOPOGRAPHIC FACTOR LS

It has been observed that soil loss per unit area increases with increasing slope length and slope steepness. The slope steepness in percent (s) and the slope length in meters (λ) are quantitatively incorporated in the USLE by the dimensionless factors S and L respectively.

The exponential dependence of soil loss on slope steepness (or gradient) is generally accepted. Mathematically the relation is:

$$E = c\ s^a$$

where E is the erosion, s the slope in percent and a is an exponent.

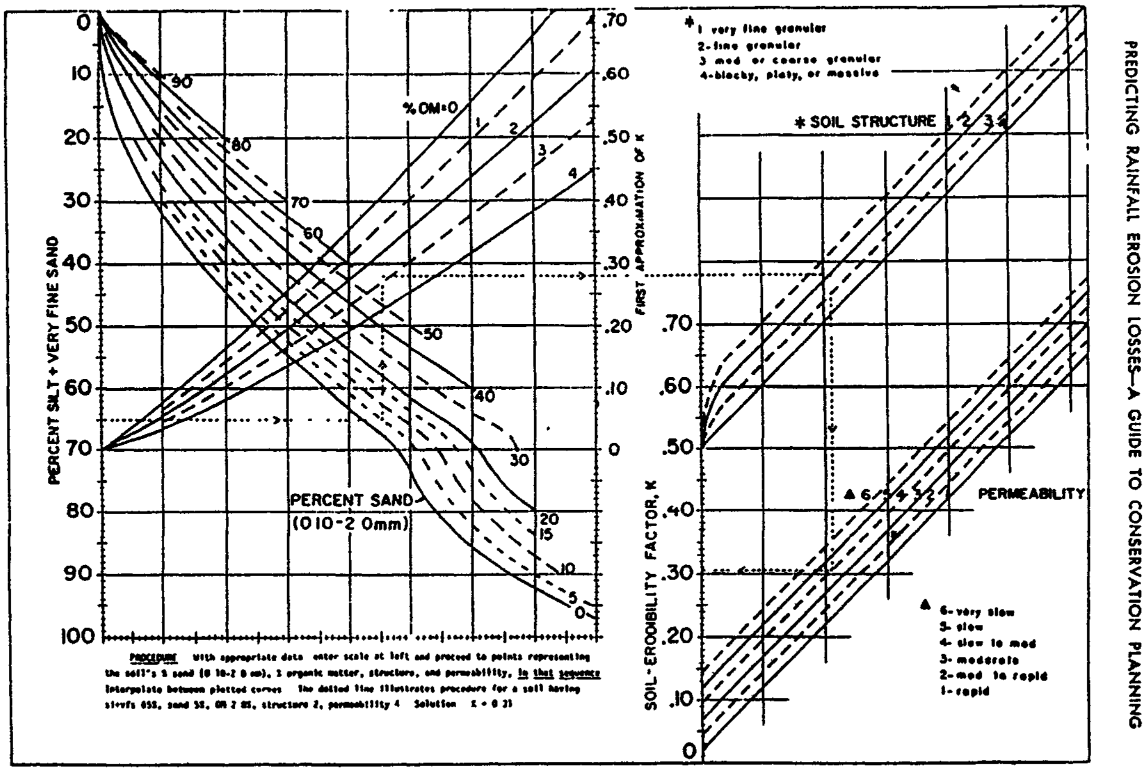

<u>Figure 2</u> : Soil erodibility nomograph (Wischmeier et al., 1971)

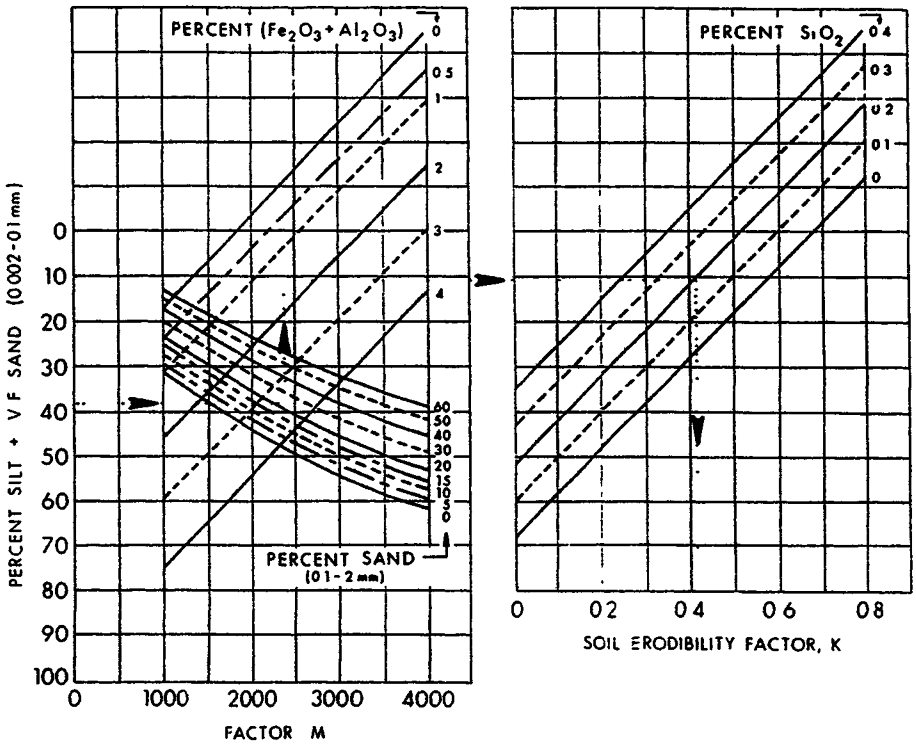

<u>Figure 3</u> : Roth, Nelson, and Romkens' (1974) nomograph for soil erodibility estimation

Zingg (1940) analyzed the results of laboratory and field plot experiments and found a value for a of 1.49. Musgrave (1947) used a = 1.35. Wischmeier and Smith (1965, 1978) calculated the dimensionless S factor for the USLE as:

$$S = \frac{0.43 + 0.30\ s + 0.043\ s^2}{6.613}$$

in which the figure 6.613 is the value of the numerator for a standard soil plot (s = 9%).

Hudson and Jackson (1959) found that in the more extreme erosion conditions of the tropics the slope effect is more exaggerated and that a figure of about 2 is more appropriate for the exponent a.

It is agreed that the dependence of soil loss E on slope length l is of the form:

$$E = b\ l^m$$

in which b and m are empirical constants. For slopes of 3 percent or less the exponent becomes 0.3, for 4 percent slopes it is 0.4, and for 5 percent or steeper the exponent is 0.5 (Wischmeier and Smith, 1958). For the USLE the slope length factor L, a dimensionless factor has been calculated as:

$$L = \left(\frac{l}{22.13}\right)^m$$

where l is the slope length in meters and 22.13 m the length for standard plots for which L = 1, and m is the exponent as explained above.

In the USLE a combined LS factor is used as shown in figure 4. This figure is intended for use on uniform slopes.

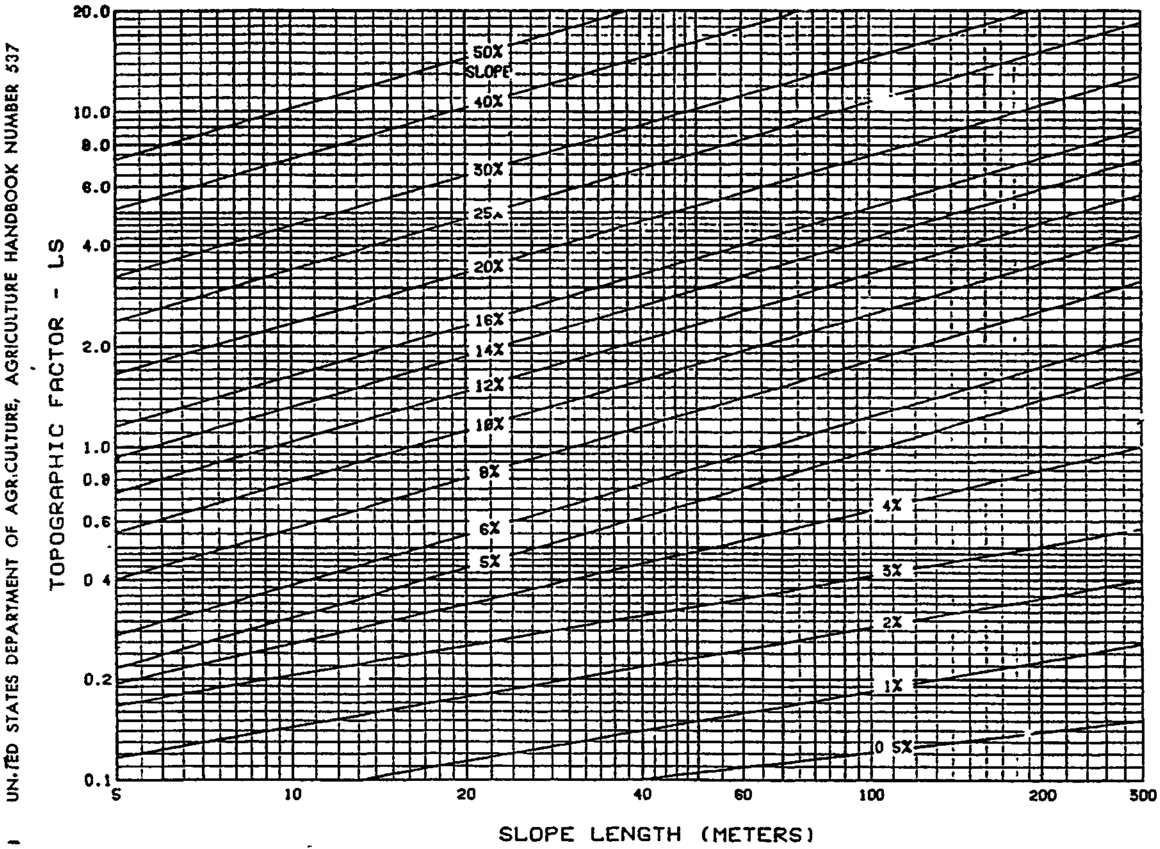

Figure 4 : Slope steepness - slope length chart

Foster and Wischmeier (1974) developed an equation to derive the LS factor for irregular slopes by breaking them up into a series of segments each with an uniform regular slope but having different gradients. Table 1 derived by this procedure shows the amounts of soil loss for successive equal-length segments of a uniform slope. Segment No. 1 is always at the top of the slope. For example, three equal length segments of a uniform 10 percent slope would be expected to produce 19, 35 and 46 percent of the loss from the entire slope.

Table 1 : Estimated relative soil losses from successive equal-length segments of a uniform slope

Number of segments	Sequence number of segment	Fraction of soil loss		
		m = 0 5	m = 0.4	m = 0.3
2	1	0.35	0.38	0.41
	2	.65	.62	.59
3	1	19	22	.24
	2	.35	35	35
	3	.46	43	41
4	1	.12	14	.17
	2	.23	.24	.24
	3	.30	.29	28
	4	.35	33	.31
5	1	.09	11	12
	2	.16	17	18
	3	.21	21	21
	4	.25	.24	.23
	5	.28	.27	.25

[1] Derived by the formula:

$$\text{Soil loss fraction} = \frac{i^{m+1} - (i-1)^{m+1}}{N^{m+1}}$$

where i = segment sequence number, m = slope-length exponent (0.5 for slopes $\geq$ 5 percent, 0 4 for 4 percent slopes, and 0.3 for 3 percent or less), and N = number of equal-length segments into which the slope was d'vided.

The following calculation illustrates the procedure for a 150 meter convex slope on which the upper third has a gradient of 5 percent; the middle third 10 percent and the lower third 15 percent.

Segment	% slope	Figure	Table	Product
1	5	1.2	0.19	0.228
2	10	3.0	0.35	1.050
3	15	5.5	0.46	2.530
			LS =	3.808

5. CROP MANAGEMENT FACTOR C

The factor C in the universal soil loss equation is the ratio of soil loss from land cropped under specific conditions to the corresponding loss from clean-tilled, continuous fallow (Wischmeier and Smith, 1978). This factor measures the combined effect of all the interrelated cover and management variables, crop sequence, productivity level, growing season length, cultural practices, residue management, rainfall distribution.

The magnitude of the C factor may be derived experimentally from research plots designed to measure soil loss. To calculate its numerical value, cropstage periods must be defined and their duration as well as cover effectiveness estimated. Each segment of the cropping and management sequence must be evaluated in combination with the rainfall erosivity distribution for the region.

To calculate the C factor, the year is divided into a series of cropstage periods defined so that cover and management effects may be considered approximately uniform within each period. Six cropstage periods were defined by Wischmeier et al. (1978):

1. Rough fallow,
2. seedbed: 10% canopy cover,
3. establishment: 50% canopy cover (35% for cotton),
4. development: 75% canopy cover (60% for cotton),
5. maturing crop,
6. residue or stubble.

Elwell and Stocking (1976) considered the time distributions of crops cover and rainfall throughout the season, and developed a percent cover-soil loss relationship as an alternative to the USLE cropping-management factor.

Table 2 reports the C factor identified by Roose (1977) for cultivated crops on Alfisols and Oxisols in West Africa.

Table 2 : Estimated value of the C factor in West Africa (Roose, 1977)

Practice	Annual average C factor
Bare soil	1
Forest or dense shrub, high mulch crops	0.001
Savannah, prairie in good condition	0.01
Over-grazed savannah or prairie	0.1
Crop cover of slow development or late planting (first year)	0.3-0.8
Crop cover of rapid development or early planting (first year)	0.01-0.1
Crop cover of slow development or late planting (second year)	0.01-0.1
Corn, sorghum, millet (as a function of yield)	0.4-0.9
Rice (intensive fertilization)	0.1-0.2
Cotton, tobacco (second cycle)	0.5-0.7
Peanuts (as a function of yield and date of planting)	0.4-0.8
First year cassava and yam (as a function of date of planting)	0.2-0.8
Palm tree, coffee, cocoa with crop cover	0.1-0.3
Pineapple on contour (as a function of slope)	
(burned residue)	0.2-0.5
(buried residue)	0.1-0.3
(surface residue)	0.01
Pineapple and tied-ridging (slope 7%)	0.1

6. CONSERVATION PRACTICE FACTOR P

The conservation practice factor or support practice factor or erosion control practice factor P in the USLE is the ratio of soil loss with a specific control practice to the soil loss with up-and-down slope culture. The erosion control practices to be considered are contouring, contour strip-cropping and terracing.

The practice factors for the three major mechanical practices as recommended by Wischmeier and Smith (1978) are shown in table 3.

Table 3 : Erosion control practice factor P (Wischmeier and Smith, 1978)

Land Slope, percentage	Contouring	Contour Strip cropping and Irrigated Furrows	Terracing(1)
1-2	0.60	0.30	0.12
3-8	0.50	0.25	0.10
9-12	0.60	0.30	0.12
13-16	0.70	0.35	0.14
17-20	0.80	0.40	0.16
21-25	0.90	0.45	0.18

(1) For prediction of contribution to off-field sediment load

The factor for terracing is for the prediction of the total off-the-field soil loss when the terrace and ridge are cropped the same as the inter-terrace area. If within terrace interval soil loss is desired, the terrace interval distance should be used for the slope length factor L.

REFERENCES

AHMAD, N. and E. BRECKNER. 1974.
Soil erosion on three Tobago soils.
Trop. Agric. (Trinidad) 51 (2): 313-324.

ARNOLDUS, H.M. 1980.
An approximation of the rainfall factor in the universal soil loss equation. In De Boodt M. and Gabriels, D. (eds.): Assessment of Erosion.
Wiley and Sons, London, pp. 127-132.

BEST, A.C. 1950.
The size distribution of raindrops.
Quaterly Journal of the Royal Meteorological Society 76, 16.

BHATIA, K.S. and R.S. SINGH. 1976.
Evaluation of rainfall intensities and erosion index values for soil conservation.
Indian For. 102 (10): 726-734.

BISAL, F. 1960.
The effect of raindrop size and impact velocity on sand splash.
Canadian Journal of Soil Science 40, 242-245.

BOLLINNE, A.; A. LAURENT; P. ROSSEAU; J.M. PAUWELS; D. GABRIELS and J. AELTERMAN 1980.
Provisional rain erosivity map of Belgium. In De Boodt, M. and D. Gabriels (eds.): Assessment of Erosion.
Wiley and Sons, Chichester, pp. 441-453.

BOLS, P.L. 1978.
The iso-erodent map of Java and Madura.
Report of the Belgian Assistance Project ATA 105, Soil Research Institute, Bogor, Indonesia.

CARTER, C.E.; J.D. GREER; H.J. BRAUD and J.M. FLOYD. 1974.
Raindrop characteristics in South Central United States.
Trans. Am. Soc. Agric. Engrs., 17, 1033-1037.

DE WULF, F. and D. GABRIELS.
A device for analyzing the energy load of raindrops. In: De Boodt, M. and D. Gabriels (eds.): Assessment of erosion.
Wiley and Sons, London, 165-169.

ELLISON, W.D. 1944.
Studies of raindrop erosion.
Agricultural Engineering, 25: 131-136, 181-182.

EL-SWAIFY, S.A. 1977.
Susceptibilities of certain tropical soils to erosion by water. In: Greenland D. and R. Lal (eds.): Soil Conservation and Management in the Humid Tropics.
Chichester, pp. 71-77.

EL-SWAIFY, S.A.; E.W. DANGLER and C.L. ARMSTRONG. 1982.
Soil erosion by water in the tropics.
Research Extension Series 024, HITAHR, College of Tropical Agriculture and Human Resources.
University of Hawaii, pp. 173.

ELWELL, H.A. and M.A. STOCKING. 1976.
Vegetal cover to estimate soil erosion hazard in Rhodesia.
Geoderma 15: 61-70.

EVANS, R. 1980.
Mechanics of water erosion. In: Kirkby M.J. and R.P. Morgan (eds.):
Soil Erosion. pp. 111.
Wiley and Sons, Chichester.

FORREST, P.M. 1970.
The development of two field instruments to measure erosivity: A simple rainfall intensity meter, and an acoustic rainfall recorder tested with a rotating disk simulator.
B. Sc. (Hons) dissertation, National College of Agricultural Engineering, Silsoc, England.

FOSTER, G.R. and W.M. WISCHMEIER. 1974.
Evaluating irregular slopes for soil loss prediction.
Trans. Amer. Soc. Agric. Eng. 17 (2): 305-309.

FOURNIER, F. 1960.
Climat et érosion.
Presses Universitaires de France, Paris.

FREE, G.R. 1960.
Erosion characteristics of rainfall.
Agr. Engr. 41: 447-449.

GUNN, R. and G.D. KINZER. 1949.
Terminal velocity of water droplets in stagnant air.
Jour. of Meteorology 6: 243-248.

HUDSON, N. and D.C. JACKSON. 1959.
Results achieved in the measurement of erosion and runoff in southern Rhodesia.
Proc. Inter. African Soils Conference Compte Rendus 3: 575-583.

HUDSON, N.W. 1963.
Raindrop size distribution in high intensity storms.
Rhodesian Journal of Agricultural Research 1, 1, 6-11.

HUDSON, N.W. 1964.
The flour pellet method for measuring the size of raindrops.
Res. Bull. No. 4, Salisbury, Rhodesia: Dept. of Conserv. and Extension.

HUDSON, N.W. 1965.
The influence of rainfall on the mechanics of soil erosion with particular reference to Southern Rhodesia.
Unpublished M.S. thesis, University of Capetown.

HUDSON, N.W. 1971.
Soil Conservation.
Ithaca, N.Y., Cornell Univ. Press.

KINNELL, P.I.A. 1968.
An acoustic impact rainfall recorder.
Postgraduate certificate dissertation, National College of Agricultural Engineering, Silsoe, England.

LAL, R. 1976.
Soil erosion on Alfisols in Western Nigeria, III: Effects of rainfall characteristics.
Geoderma 16: 389-401.

LAWS, J.O. 1941.
Measurements of fall-velocity of waterdrops and raindrops.
Trans. Amer. Geophys. Union 22: 709-712.

LAWS, J.O. and D.A. PARSONS. 1943.
The relation of raindrop size to intensity.
Trans. Amer. Geophys. Un. 24: 452-459.

MIHARA, J. 1952.
Raindrops and soil erosion.
Nation. Inst. Agric. Sci., Tokyo, Japan.

MIHARA, H. 1959.
Raindrops and soil erosion.
Bulletin of the National Institute of Agricultural Science, Series A, 1.

MUSGRAVE, G.W. 1947.
The quantitative evaluation of factors in water erosion, a first approximation.
Jour. Soil and Water Conservation 2: 133-138.

ROOSE, E. 1977.
Application of the universal soil loss equation of Wischmeier and Smith in West Africa. In Greenland and Lal (eds.): Soil conservation and management in the humid tropics.
Wiley and Sons, London, pp. 177-187.

ROTH, C.B.; D.W. NELSON and M.J. ROMKENS. 1974.
Prediction of subsoil erodibility using chemical, mineralogical, and physical parameters.
EPA-660/2-74-043, Washington, D.C., U.S. Environmental Protection Agency, Office of Research and Development.

WISCHMEIER, W.H. and D.D. SMITH. 1958.
Rainfall energy and its relationship to soil loss.
Trans. Amer. Geophys. Union 39 (2): 285-291.

WISCHMEIER, W.H. and D.D. SMITH. 1965.
Predicting rainfall-erosion losses from cropland east of the Rocky Mountains.
Agric. Handbook No. 282, Washington, D.C., USDA.

WISCHMEIER, W.H. and J.V. MANNERING. 1969.
Relation of soil properties to its erodibility.
Proc. Soil Sci. Soc. Amer. 33 (1): 131-137.

WISCHMEIER, W.H.; C.B. JOHNSON and B.V. CROSS. 1971.
A soil erodibility nomograph for farmland and construction sites.
Jour. of Soil and Water Conservation 26 (5): 189-193.

WISCHMEIER, W.H. and D.D. SMITH. 1978.
Predicting rainfall-erosion losses. A guide to conservation planning.
Agric. Handbook No. 537. Washington, D.C., USDA.

ZINGG, A.W. 1940.
Degree and length of land slope as it affects soil loss in run-off.
Agric. Eng. 21: 59-64.

Chapter 1

Model Structures

A model is a description of the physical reality using mathematical equations. The origin of these equations will determine the general model concept: the two basic model structures are *theoretical* and *experimental.*

The theoretical model structure is also called conceptual. In this method, the modelled system is described by the basic physical laws (equilibrium equations, conservation of mass and energy, etc...) which determine the system behaviour. Depending on the complexity of the processes one wants to model, there are almost always simplifications necessary in order to make the calculations practicable. Many systems are not only time-dependent, but also space dependent. Such systems are systems with *distributed* parameters, and their corresponding models are then called distributed models. Usually, these models are simplified by *lumping*: the physical equations are only applied on some points in space.

The experimental model structure is also called black-box or empirical. In this structure, the model is derived from measurements. Starting from a theoretical analysis, the input and output variables are measured. These measurements are used to find mathematical relations between the measured variables. A difficult task is the elimination of disturbing influences, which may result in erroneous measurements.

Both theoretical and experimental models have their advantages and disadvantages. However, a huge advantage of the theoretical model structure is that the mathematical relation is conserved between the system parameters and the physical parameters of the processes. In experimental models these relations are lost, the system parameters are then just numbers without a physical meaning. When the system becomes more complex, it becomes more and more difficult to implement a theoretical model. This is a drawback not occurring in the experimental methodology.

In both theoretical and experimental methods, one can make a distinction between *stochastic* and *deterministic* models. A model is stochastic if one or more system parameters are random variables. This means that the exact value of that parameter can not be determined. In natural systems such variables are abundant (e.g. the daily amount of rainfall, the length of the daily queues on the motor ways, etc...). Probably, almost all physical, social and economic parameters have a stochastic nature. In some cases, these fluctuations are not important and are not taken into account. Then, one can say that these parameters are quasi-deterministic. Consider the output variable $y(t)$ of a dynamical system with as input variable $u(t)$. When the value of $y(t)$ can be exactly derived from the system behaviour and from the input variable $u(t)$, then we can say that $y(t)$ is a deterministic system. It is then possible to make the following division concerning the model structure (Clarke, 1973):

1. stochastic-theoretical
2. stochastic-experimental
3. deterministic-theoretical
4. deterministic-experimental

These four groups can then be further extended in:

1. linear systems
2. nonlinear systems

When the output signal $y_1(t)$ corresponds with the input $u_1(t)$ and $y_2(t)$ corresponds with the input $u_2(t)$, then the system is called linear when $y_1(t) + y_2(t)$ corresponds with $u_1(t) + u_2(t)$ (superposition principle). This linearity may not be confused with the linearity in statistical (regressions) sense.

Chapter 2

Infiltration Processes

2.1 Infiltration processes

Infiltration is the process of water penetrating from the ground surface into the soil. Many factors influence the infiltration rate, including the condition of the soil surface and its vegetation cover, the properties of the soil, such as its porosity and hydraulic conductivity, and the initial moisture content of the soil. Soil strata with different physical properties may overlay each other, forming horizons. Also, soil exhibits a large spatial variability even within relatively small areas such as a field. As a result of these spatial and time variations in soil properties, infiltration is a very complex process. Consequently, it can be described only approximately with mathematical equations (Chow et al., 1988). These mathematical equations can be subdivided into two main groups: the Green-Ampt (Green and Ampt, 1911) and the Richards equations (Richards, 1931). Remark that these references might look 'old'. However, it is only now, with the processing capacity of modern computers, that the power of these equations can be fully exploited inside distributed hydrological models.

2.2 Units

Table 2.1 gives an overview of the SI units used in soil physics. To convert from the SI units to the indicated units, multiply by the indicated value

Table 2.1: *Conversion factors for commonly used units in soil physics*

Quantity	**SI units**	**Equivalent units**
water potential	$1\ J \cdot kg^{-1}$	0.102 meters of water
water potential	$1\ J \cdot kg^{-1}$	1 kPa
water potential	$1\ J \cdot kg^{-1}$	0.01 bar
water flux density	$1\ kg \cdot m^{-2} \cdot s^{-1}$	$1\ mm \cdot s^{-1}$
hydraulic conductivity	$1\ kg \cdot s \cdot m^{-3}$	$58.8\ cm \cdot min^{-1}$

2.3 Infiltration during unsteady rainfall events

Most rain events, if not all, have an unsteady character: there are multiple periods of infiltration during surface ponding and infiltration without surface ponding. Under a ponded surface the infiltration process is independent of the effect of time distribution of rainfall. The rate of infiltration reaches its maximum capacity and is referred to as the infiltration capacity. Without surface ponding, all the rainfall infiltrates into the soil. The infiltration models described in the previous sections describe infiltration during ponding. If the time that separates the two stages can be determined, the difficulty involved in modelling infiltration during an unsteady rainfall event is reduced, since the infiltration for different stages can be treated separately.

One such methodology to simulate infiltration during unsteady rainfall events is the 'time compression approximation' (Ibrahim and Brutsaert, 1968), which can be used in combination with any infiltration model. This method implies the knowledge of the infiltration characteristic of the soil. Figure 2.1 shows the general concept of the time compression approximation. If the soil infiltration characteristic is superimposed with the first part of cumulative rainfall curve, then the portion which will infiltrate can be estimated graphically: at time t_1 a portion I_1 will infiltrate. The second part of the cumulative rainfall curve should be superimposed at I_1. The third part of the cumulative rainfall curve is superimposed at I_2. Finally, the fourth part is superimposed at I_3. During the second and fourth time interval, no runoff is generated.

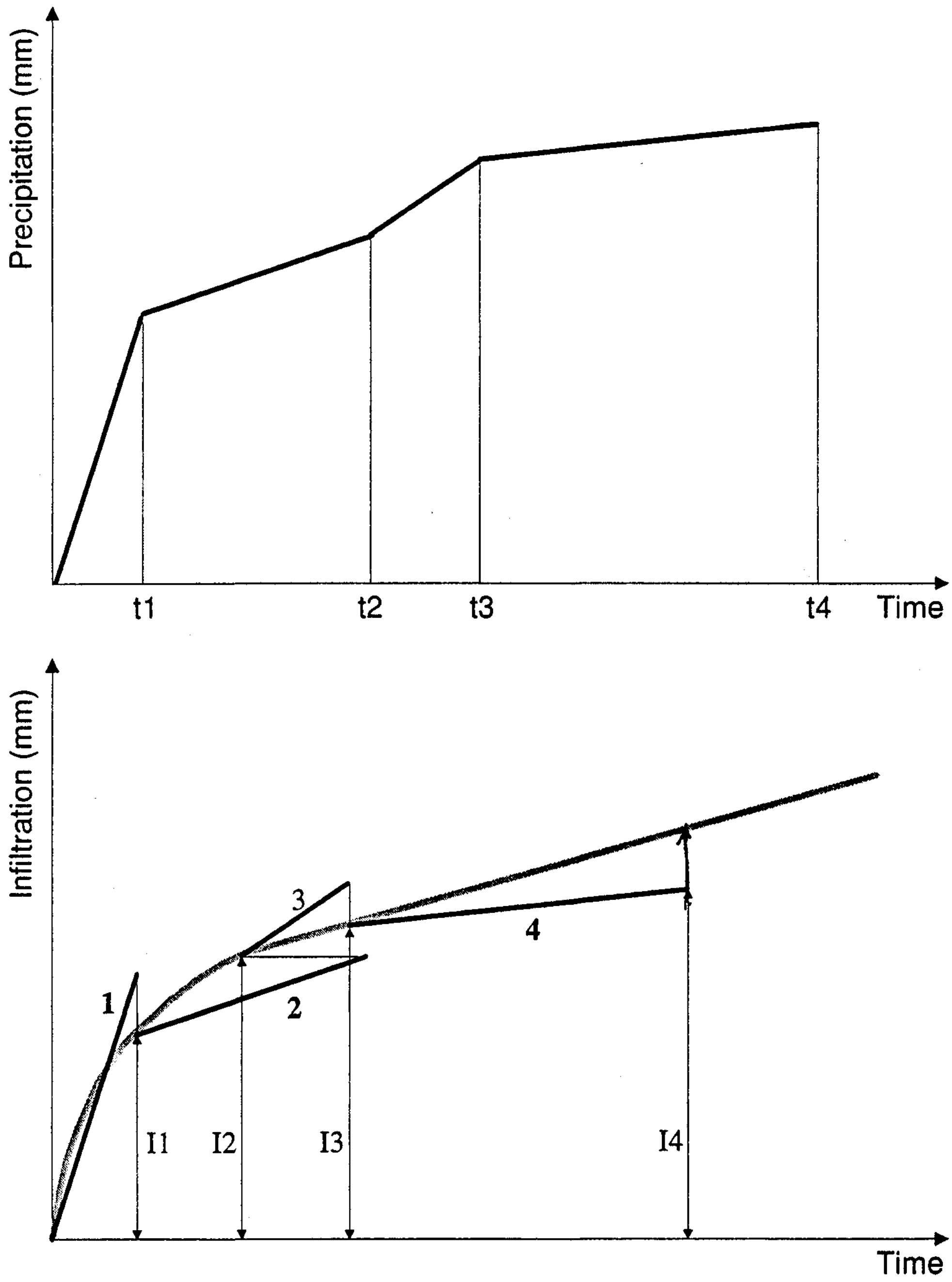

Figure 2.1: *The top graph shows the cumulative precipitation of an unsteady rain event. The bottom graph shows the time compression approximation concept, wherein the grey line is the soil infiltration characteristic.*

2.4 Determination of the soil infiltration characteristic

For accurate infiltration/runoff modelling, it is necessary to derive the soil specific infiltration characteristic from field measurements ! However, when the infiltration/runoff has to be determined on homogeneous soils (soils without crack formation, stones, vertic properties and with a deep homogenous soil profile, e.g. the Luvisols of Western Europe) the infiltration characteristic can be determined using the Green-Ampt concept:

the wetting front is a sharp boundary dividing the soil of initial moisture content (θ_i, $m \cdot m^{-3}$) below from saturated soil with moisture content (θ_s, $m \cdot m^{-3}$) above. The basic infiltration equation is based on the Darcy equation (Schmidt, 1996):

$$i = -K_s \cdot \frac{\Delta(\Psi_m + \Psi_g)}{x_{wf}(t)} \tag{2.1}$$

wherein, i is the infiltration rate ($kg \cdot s \cdot m^{-3}$), K_s is the saturated hydraulic conductivity ($kg \cdot s \cdot m^{-3}$), Ψ_m the matric potential ($J \cdot kg^{-1}$), Ψ_g the gravitational potential ($J \cdot kg^{-1}$) and $x_{wf}(t)$ the depth of the wetting front (m) at time t. This infiltration equation can be further simplified by supposing:

$$\Delta\Psi_m \approx \Psi_{mi} \tag{2.2}$$

with, Ψ_{mi} the matric potential at the initial water content θ_i. Equation (2.1) is composed of a stationary and instationary component. The stationary component is:

$$i_1 = -K_s \cdot \frac{\Delta\Psi_g}{x_{wf1}} = -K_s \cdot g = \rho_w \cdot \Delta\theta \cdot \frac{dx_{wf1}}{dt} \tag{2.3}$$

wherein, g is the gravitational constant ($m \cdot s^{-2}$), ρ_w is the water density ($kg \cdot m^{-3}$), and $\Delta\theta = \theta_s - \theta_i$. Integrating equation (2.3) results in:

$$x_{wf1} = -\frac{K_s \cdot g \cdot t}{\rho_w \cdot \Delta\theta} \tag{2.4}$$

The instationary component is:

$$i_2 = -K_s \cdot \frac{\Psi_{mi}}{x_{wf2}} = \rho_w \cdot \Delta\theta \cdot \frac{dx_{wf2}}{dt} \tag{2.5}$$

Integrating this equation results in:

$$x_{wf2} = -\sqrt{\frac{2 \cdot K_s \cdot \Psi_{mi} \cdot t}{\rho_w \cdot \Delta\theta}} \tag{2.6}$$

The depth of the wetting front is the result of both the stationary and unstationary component:

$$x_{wf} = -\left(\frac{K_s \cdot g \cdot t}{\rho_w \cdot \Delta\theta} + \sqrt{\frac{2 \cdot K_s \cdot \Psi_{mi} \cdot t}{\rho_w \cdot \Delta\theta}}\right) \tag{2.7}$$

All parameters in equation (2.1), which is used to determine the soil specific infiltration characteristic, are now determined. To apply this infiltration model in practice, the following data are necessary:

1. the saturated hydraulic conductivity
2. the water retention characteristic of the soil.

Remark that this methodology ONLY applies for HOMOGENEOUS soil profiles. If this is not the case, the soil specific infiltration characteristic has to be determined from field experiments !

2.4.1 Estimation of the saturated hydraulic conductivity

The saturated hydraulic conductivity (K_s) can be estimated if the soil texture and soil density of the soil are known. A frequently used equation to estimate K_s is (Campbell, 1985):

$$K_s = 0.004 \cdot \left(\frac{1.3}{\rho_s}\right)^{1.3 \cdot b} \cdot e^{-6.9 \cdot m_c - 3.7 \cdot m_s} \tag{2.8}$$

wherein m_c is the clay $(0 - 2\ \mu m)$ mass fraction $(kg \cdot kg^{-1})$, m_s is the silt $(2 - 50\ \mu m)$ mass fraction $(mass \cdot mass^{-1})$, and ρ_s is the density of the soil $(ton \cdot m^{-3})$. In this equation, K_s is expressed in $(kg \cdot s \cdot m^{-3})$. To convert this to $(m \cdot h^{-1})$, equation (2.8) must be multiplied with 35.28. The parameter b is a function of the 'air entry' water potential, ψ_{es} $(J \cdot kg^{-1})$, and the standard deviation of the geometric diameter of the soil particles, σ_g, according to:

$$b = (-2 \cdot \psi_{es}) + (0.2 \cdot \sigma_g) \tag{2.9}$$

The air entry water potential is the water pressure in a capillary tube beneath the meniscus. When the water pressure becomes lower than the air entry water potential then the capillary tube cannot retain the water anymore. The air entry water potential of a certain soil can be estimated with:

$$\psi_{es} = -0.5 \cdot (d_g)^{-0.5} \tag{2.10}$$

where d_g is the geometric diameter of the soil particles (mm). The geometric diameter and the geometric standard deviation can be calculated using (Shirazi and Boersma, 1984):

$$d_g = exp\left(\sum_n F_n \cdot ln(d_n)\right) \tag{2.11}$$

$$\sigma_g = exp\left(\sqrt{\left(\sum_n F_n \cdot (ln(d_n))^2\right) - \left(\sum_n F_n \cdot ln(d_n)\right)^2}\right) \tag{2.12}$$

wherein, n is the number of textural classes, F_n is the mass fraction of textural fraction n ($kg \cdot kg^{-1}$), and d_n the mean diameter of textural fraction n (mm).

2.4.2 Estimation of the water retention characteristic

The knowledge of the water retention characteristic is essential to describe water movement through a soil profile. The determination of the water retention characteristic consists of measuring the soil water content at given suction levels. A continuous curve is then fitted through the measurements. The best known and most frequently used curve, is the Van Genuchten model (Van Genuchten, 1980):

$$\theta = \theta_r + \frac{\theta_s - \theta_r}{(1 + (\alpha \cdot h)^n)^m} \tag{2.13}$$

In this equation α, n and $m(= 1 - 1/n)$ have no physical meaning and determine the general form of the curve. θ_s is the moisture content at saturation ($cm^3 \cdot cm^{-3}$), θ_r is the residual moisture content at a pF of 4.2 ($cm^3 \cdot cm^{-3}$) and h is the matric potential ($cm\ H_2O$). Because m and n are not independent, m can be set to equal 1, such that equation (2.13) can be simplified to a function of four parameters ($\theta_s, \theta_r, \alpha, n$). Rewriting equation (2.13) results in:

$$h(\theta) = \left(\left(\left(\frac{\theta_s - \theta_r}{\theta - \theta_r} \right) - 1 \right) \cdot \frac{1}{\alpha^n} \right)^{\frac{1}{n}} \tag{2.14}$$

The four parameters of this equation ($\theta_s, \theta_r, \alpha, n$) can be estimated using the pedotransfer functions of Vereecken et al. (1989):

$$\theta_s = 0.81 - (0.283 \cdot \rho_s) + (0.001 \cdot Cl) \tag{2.15}$$

$$\theta_r = 0.015 + (0.005 \cdot Cl) + (0.014 \cdot C) \tag{2.16}$$

$$\alpha = exp(-2.486 + (0.025 \cdot Sa) - (0.351 \cdot C) - (2.617 \cdot \rho_s) - (0.023 \cdot Cl)) \tag{2.17}$$

$$n = exp(0.053 - (0.009 \cdot Sa) - (0.013 \cdot C) + (0.00015 \cdot Sa^2) \tag{2.18}$$

wherein, ρ_s is the soil density ($g \cdot cm^{-3}$), Cl is the clay content (%), Sa is the sand content (%) and C is the organic carbon content (%). These regression equations were derived from Belgian soil types and have an adjusted R squared value of respectively: 84.8, 70.3, 68.0 and 56.0. With these equations the water retention characteristic can be estimated based on the texture, organic carbon content and the soil density.

Chapter 3

Overland Flow Processes

3.1 Distributed flow routing: the Saint-Venant equations

The flow of water over the land, through the soil and in stream channels of a watershed is a distributed process because the flow rate, flow velocity and flow depth vary in space throughout the watershed. Estimates of flow rate and/or water level at important locations in the channel can be obtained using a distributed flow routing model. This type of model is based on the partial differential equations (the Saint-Venant equations for one-dimensional flow) that allow the flow rate and water level to be computed as function of space and time, rather than time alone, as in the lumped models. The flow processes in natural hydrological systems vary in all three space dimensions. However, for many practical situations, the spatial variation of velocity across the channel and with respect to the depth can be ignored, so that the flow process can be approximated by a one-dimensional model. The Saint-Venant equations (de Saint-Venant, 1871) describe a one-dimensional unsteady open channel flow. Because the Saint-Venant equations form the basis of almost all physical flow routing models the mathematical background of these equations is given here.

Consider an elementary channel segment (figure 3.1), with a length dx and a small time interval dt. Then, based on the principle of mass conservation, one can write:

$$\frac{\partial S}{\partial t} \cdot dt = Q \cdot dt - \left(Q + \frac{\partial Q}{\partial x} \cdot dx\right) \cdot dt. \tag{3.1}$$

In this equation is S the storage in the control volume, $Q(x,t)$ the segment inflow and

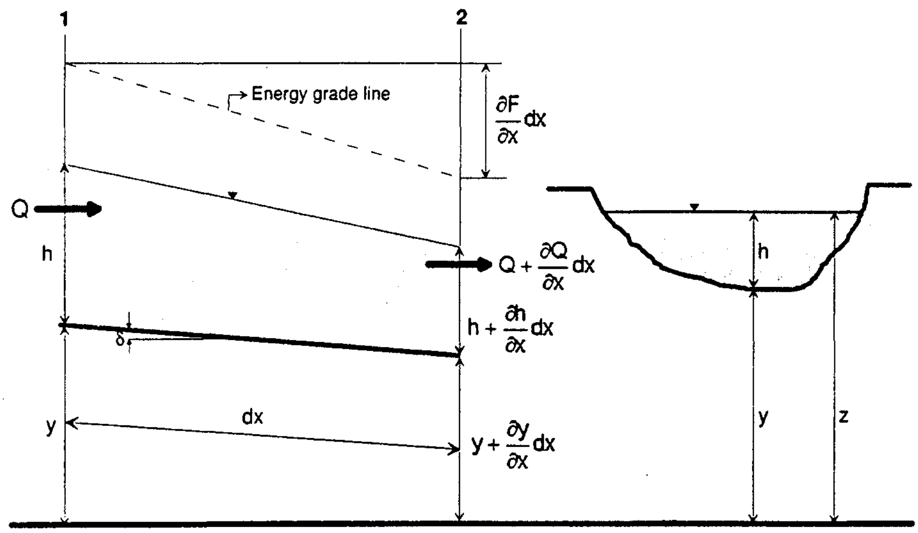

Figure 3.1: *Elementary channel segment.*

$Q + ((\partial Q/\partial x) \cdot dx)$ the segment outflow. Consider A the cross-sectional area, then is $S = A \cdot dx$ and consequently:

$$\frac{\partial S}{\partial t} = \frac{\partial A}{\partial t} \cdot dx \tag{3.2}$$

thus:

$$\frac{\partial A}{\partial t} \cdot dx \cdot dt = -\frac{\partial Q}{\partial x} \cdot dx \cdot dt \tag{3.3}$$

the continuity equation then becomes:

$$\frac{\partial Q}{\partial x} + \frac{\partial A}{\partial t} = 0. \tag{3.4}$$

The second basic equation is based on the energy balance. Applying the Bernoulli equation on the elementary channel section gives:

$$\Delta_1^2 \left(z + \frac{p}{\rho \cdot g} + \alpha \cdot \frac{v^2}{2 \cdot g} + \frac{1}{g} \cdot \int_x^{x+dx} \frac{\partial v}{\partial t} \cdot dx + F \right) = 0 \tag{3.5}$$

wherein, z is the elevation of the water level (m), p the pressure ($N \cdot m^{-2}$), ρ is the fluid density ($kg \cdot m^{-3}$), g the gravitational constant ($m \cdot s^{-2}$), α the Coriolis coefficient ($-$), v the mean velocity of the flow ($m \cdot s^{-1}$), and F the hydraulic head (m). Consider a constant hydrostatical pressure in every cross-section ($z + p/\rho g$ is constant) and for a point at the surface is $p = p_{atmospherical} = 0$. Consider also a turbulent flow, so that $\alpha \approx 1$. Equation (3.5) can then be rewritten as:

$$\Delta_1^2 \left(z + \frac{v^2}{2 \cdot g} + \frac{1}{g} \cdot \int_x^{x+dx} \frac{\partial v}{\partial t} \cdot dx + F \right) = 0. \tag{3.6}$$

By dividing with x, using the $\lim_{dx \to 0}$ operator and by considering a constant t:

$$\frac{\partial z}{\partial x} + \frac{\partial}{\partial x} \left(\frac{v^2}{2 \cdot g} \right) + \frac{1}{g} \cdot \frac{\partial}{\partial x} \left(\int_x^{x+dx} \frac{\partial v}{\partial t} \cdot dx \right) + \frac{\partial F}{\partial x} = 0 \tag{3.7}$$

or:

$$\frac{\partial z}{\partial x} + \frac{\partial}{\partial x} \left(\frac{v^2}{2 \cdot g} \right) + \frac{1}{g} \cdot \frac{\partial v}{\partial t} + S_f = 0 \tag{3.8}$$

with $S_f = \partial F / \partial x$ the head loss per unit length. Introducing the water level h in replacement of the elevation z, with $z = y + h$, results in:

$$\frac{\partial z}{\partial x} = \frac{\partial y}{\partial x} + \frac{\partial h}{\partial x} \tag{3.9}$$

and with:

$$\frac{\partial y}{\partial x} = -sin(\delta) \approx -S_0 \tag{3.10}$$

wherein S_0 is the local bed slope, with δ having small values. Equation (3.8) can then be written as:

$$-S_0 + \frac{\partial h}{\partial x} + \frac{\partial}{\partial x} \left(\frac{v^2}{2 \cdot g} \right) + \frac{1}{g} \cdot \frac{\partial v}{\partial t} + S_f = 0. \tag{3.11}$$

The latter equation can also be written in terms of the dependent variables Q (discharge) and h (water level). Taking into account that $Q = v \cdot A$, and v perpendicular on A (thus, for small bed slopes S_0), equation (3.11) becomes:

$$\frac{\partial Q}{\partial t} + \frac{\partial}{\partial x} \left(\frac{Q^2}{A} \right) = A \cdot \left(\frac{\partial v}{\partial t} + \frac{1}{2} \cdot \frac{\partial v^2}{\partial x} \right) \tag{3.12}$$

$$S_f = S_0 - \frac{\partial h}{\partial x} - \frac{1}{g \cdot A} \cdot \frac{\partial Q}{\partial t} - \frac{1}{g \cdot A} \cdot \frac{\partial}{\partial x}\left(\frac{Q^2}{A}\right) \tag{3.13}$$

The momentum equation can then be written as:

$$\underbrace{\frac{1}{A} \cdot \frac{\partial Q}{\partial t} + \frac{1}{A} \cdot \frac{\partial}{\partial x}\left(\frac{Q^2}{A}\right) + \underbrace{g \cdot \frac{\partial h}{\partial x} - \underbrace{g \cdot (S_0 - S_f)}_{Kinematic\ wave}}_{Diffusion\ wave}}_{Dynamic\ wave} = 0. \tag{3.14}$$

Equation (3.4) forms together with equation (3.14) the Saint-Venant equations. In equation (3.14) the terms are respectively: the local acceleration term, the convective acceleration term, the pressure force term, the gravity force term and the friction force term.

3.2 Overland flow routing model

The simplest distributed model is the kinematic wave model, which neglects the local acceleration, convective acceleration and pressure terms in the momentum equation. It assumes $S_0 = S_f$ and the friction and gravity forces balance each other. The diffusion wave model neglects the local and convective acceleration terms but incorporates the pressure term. The dynamic wave model considers all the acceleration and pressure terms in the momentum equation. Kinematic waves govern flow when inertial and pressure forces are not important. Dynamic waves govern flow when these forces are important, such as in the movement of a large flood wave in a wide river. For a kinematic wave motion, the Saint-Venant equations reduce to (Chow et al., 1988):

$$\frac{\partial Q}{\partial x} + \frac{\partial A}{\partial t} = q \quad \textit{continuity equation} \tag{3.15}$$

$$S_0 = S_f \quad \textit{momentum equation} \tag{3.16}$$

wherein S_f is the friction slope and supposed to be equal to the bed slope, S_0 $(m \cdot m^{-1})$, q is the lateral inflow per unit width $(m^3 \cdot s^{-1} \cdot m^{-1})$, A is crossectional flow area (m^2) and Q is the discharge $(m^3 \cdot s^{-1})$. The momentum equation can also be represented by (Chow et al., 1988):

$$A = \alpha \cdot Q^{\beta}. \tag{3.17}$$

Based on the Manning equation, with $S_f = S_0$ and $R = A/P$ (R is the hydraulic radius and P the wetted perimeter) the following relation can be found:

$$Q = \frac{\sqrt{S_0}}{n \cdot P^{2/3}} \cdot A^{5/3} \tag{3.18}$$

with n the Manning roughness coefficient ($s \cdot m^{-1/3}$). This last equation can be solved for A:

$$A = \left(\frac{n \cdot P^{2/3}}{\sqrt{S_0}}\right)^{3/5} \cdot Q^{3/5}. \tag{3.19}$$

The parameters α and β in equation (3.17) are then:

$$\alpha = \left(\frac{n \cdot P^{2/3}}{\sqrt{S_0}}\right)^{0.6} \tag{3.20}$$

$$\beta = 3/5 = 0.6 \tag{3.21}$$

For a broad overland flow, P equals the hillslope segment width, B. Equation (3.15) has two dependent parameters: A and Q. A can be eliminated by differentiating equation (3.17) and by substituting the term $\partial A/\partial t$ in equation (3.15). This results in:

$$\frac{\partial Q}{\partial x} + \alpha \cdot \beta \cdot Q^{\beta-1} \cdot \frac{\partial Q}{\partial t} = q \tag{3.22}$$

In order to calculate the net erosion and deposition along a hillslope, it is necessary to know the hydrographs of every hillslope segment. To determine these hydrographs, equation (3.22) can be solved using a finite difference numerical method (figure 3.2). The objective of the numerical solution is to solve equation (3.22) for $Q(x,t)$ at each point on the x–t grid, given the channel parameters α, β, the lateral inflow $q(t)$ and the initial and boundary conditions. In particular, the purpose of the solution is to determine the outflow hydrograph of a certain hillslope segment.

The numerical solution of the kinematic wave equation is more flexible than the analytical, it is more easy to handle variations in the channel properties and in the initial and boundary conditions, and serves as an introduction to numerical solution of the dynamic wave equation (which can be implemented in future versions of the STM-2D/3D model). Equation (3.22) can be written as, with i and j variables indicating respectively the hillslope or channel segment and the time step:

$$\frac{Q_{i+1}^{j+1} - Q_{i}^{j+1}}{\Delta x_i} + \alpha\beta\left(\frac{Q_{i+1}^{j} + Q_{i}^{j+1}}{2}\right)^{\beta-1}\left(\frac{Q_{i+1}^{j+1} - Q_{i+1}^{j}}{\Delta t}\right) = \frac{q_{i+1}^{j+1} + q_{i+1}^{j}}{2} \tag{3.23}$$

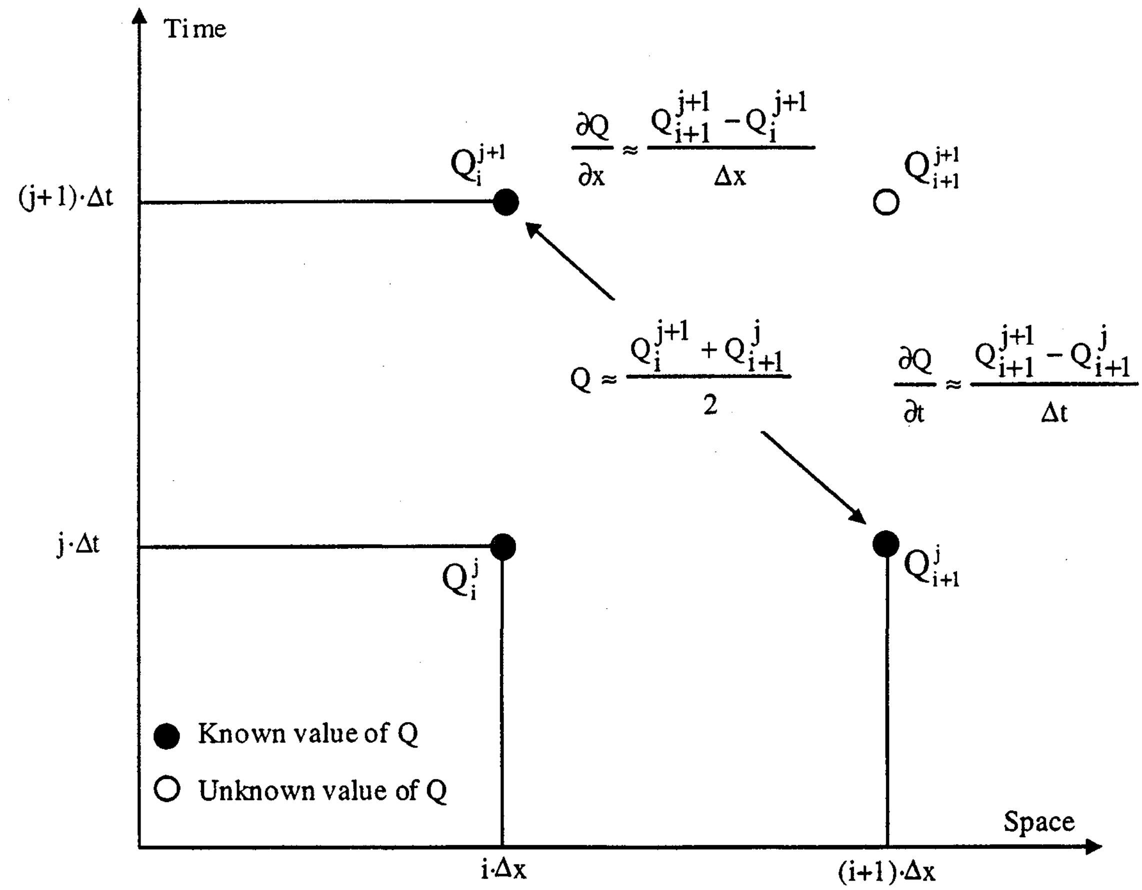

Figure 3.2: *Implicit linear finite difference scheme for solution of the kinematic wave equation (Chow et al., 1988).*

Equation (3.23) can now be solved for the unknown Q_{i+1}^{j+1}, with Δx_i the length of a segment i (m):

$$Q_{i+1}^{j+1} = \frac{\frac{\Delta t}{\Delta x_i} Q_i^{j+1} + \alpha\beta Q_{i+1}^{j} \left(\frac{Q_{i+1}^{j}+Q_i^{j+1}}{2}\right)^{\beta-1} + \Delta t \left(\frac{q_{i+1}^{j+1}+q_{i+1}^{j}}{2}\right)}{\frac{\Delta t}{\Delta x_i} + \alpha\beta \left(\frac{Q_{i+1}^{j}+Q_i^{j+1}}{2}\right)^{\beta-1}} \tag{3.24}$$

To solve equation (3.24) three boundary conditions must be known: (1) the maximum length of a time step to ensure accurate calculations (applies only to explicit schemes), (2) the upstream boundary condition $Q(0,t)$ and (3) the lateral inflow $q(t)$.

For a given precipitation event and soil parameters, the Green-Ampt runoff volume, $Q(GA)$, can be calculated. The water level, h (m), and the wave celerity, Ck $(m \cdot s^{-1})$, can be calculated using the following equations:

$$h_i^j = \left(\frac{n_i \cdot Q(GA)_i^j}{\sqrt{S_{0i}} \cdot B_i}\right)^{3/5} \tag{3.25}$$

$$Ck_i^j = \left(\frac{5}{3}\right) \cdot \left(\frac{\sqrt{S_{0i}}}{n_i}\right) \cdot \left(h_i^j\right)^{2/3} \tag{3.26}$$

wherein B is the width of the flow (m), and in the case of a broad overland flow (sheet flow) B equals the width of a segment.

A necessary condition for the stability of the numerical algorithms is that the time step of an explicit finite difference routine must be small enough (the Courant condition), according to (Courant and Friedrichs, 1948):

$$\Delta t \leq minimum \left(\frac{\Delta x_i}{Ck_i^j}\right). \tag{3.27}$$

This condition requires that the time step is smaller than the time for a wave to travel the distance Δx_i. If Δt is so large that the Courant condition is not satisfied, then there is an accumulation or piling up of water. The Courant condition does not apply for implicit schemes, like the one shown in figure 3.2. Figure 3.3 shows two hydrographs at the outlet of a straight rectangular shaped channel with a uniform slope of 5 %, and 10 segments of each 30 meter. The hydrograph at the upper boundary is known and the hydrographs are calculated using an implicit linear finite difference scheme of the kinematic wave, with time steps of 76 s (the Courant condition) and 300 s (a timestep 4 times larger than the Courant condition). From this figure, it can be concluded that the general shape of the outlet hydrograph is not dependent on the time step of the calculations in an implicit scheme. However, the larger the time step, the less accurate the peak discharge is determined. Therefore, it is advisable not to chose the time step too large.

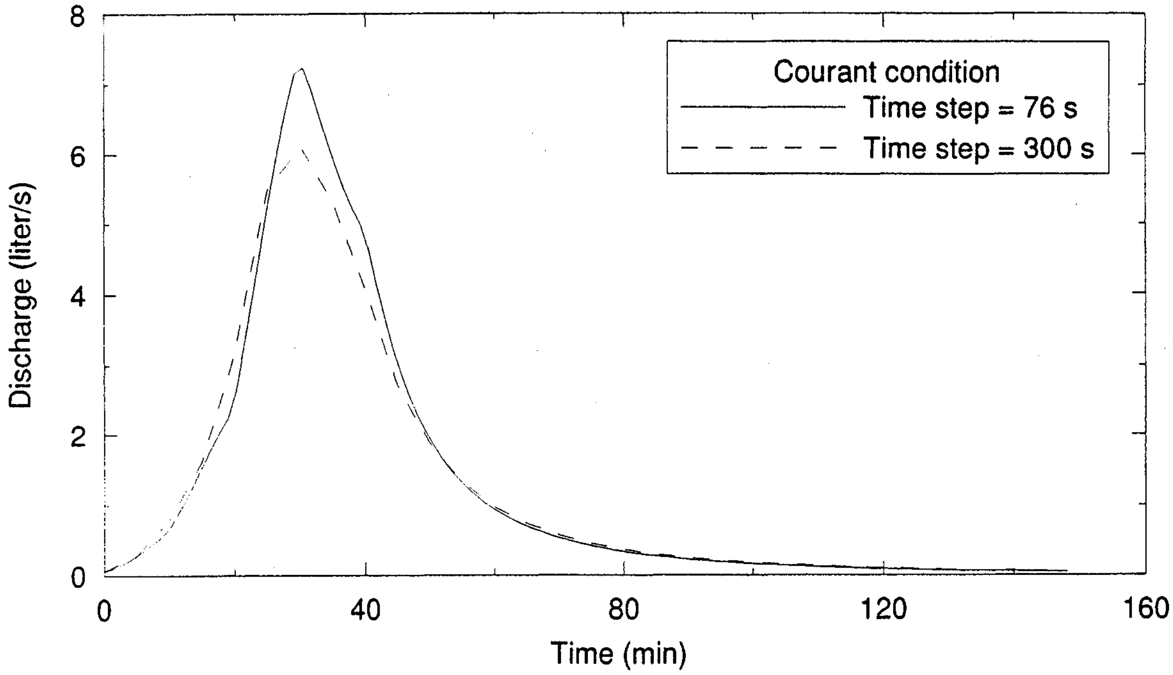

Figure 3.3: *Two hydrographs at the channel outlet for a given upstream wave. The channel has a uniform slope of 5 % and consists of 10 segments, each 30 m long. The hydrographs were calculated using a linear implicit finite difference scheme of the kinematic wave equation. The time step of the calculations was 76 s (the Courant condition) and 300 s.*

3.3 Boundary conditions for the overland flow

The upstream (at segment $i = 1$) boundary condition for an overland runoff flowline can be written as:

$$Q_1^j = Q(TCA)_1^j \tag{3.28}$$

with $Q(TCA)$ the runoff amount determined with the Green-Ampt infiltration model in combination with the time compression algorithm (TCA). The lateral inflow can then be quantified with:

$$q_i^j = \frac{Q(TCA)_i^j}{\Delta x_i} \tag{3.29}$$

3.4 Estimating the Manning roughness coefficient

Chow (1959) reported mean values for the Manning roughness coefficients for pasture, field crops, light brush and weeds, dense brush, and dense trees are respectively: 0.035, 0.040, 0.050, 0.070 and 0.100.

Chapter 4

Sediment Transport Processes

For the erosional processes in rills and gullies, Nearing et al. (1997) reported a simple but very accurate transport function. Based on laboratory flume experiments (soil in V-shaped flumes was exposed to a known discharge) using silt loam and sandy loam soils, these authors found a single logistic relationship ($R^2 = 0.93$) between the unit sediment load and the stream power of the overland flow, for all soil types (see figure 4.2). This indicates that for all unconsolidated agricultural soils in the Belgian loess belt the same transport function can be used. The stream power can be calculated with:

$$\omega = \rho_w \cdot g \cdot S \cdot q \tag{4.1}$$

wherein ρ_w is the density of water ($g \cdot cm^{-3}$), g is the gravitational constant ($cm \cdot s^{-2}$), S is the slope ($m \cdot m^{-1}$) and q is the discharge per unit width ($cm^2 \cdot s^{-1}$). The resulting rill transport equation can be written as:

$$log_{10}(q_s) = a + b \cdot \frac{e^{c+d \cdot log_{10}(\omega)}}{(1 + e^{c+d \cdot log_{10}(\omega)})} \tag{4.2}$$

with parameters $a = -34.47$, $b = 38.61$, $c = 0.845$, $d = 0.412$. From their experiments it was found that for slopes lower than 30 %, transport capacity was already reached within the first 180 cm of rill length.

Although the most important transport of soil particles towards the drainage system is governed by rill flow, sheet erosion processes in the interrill areas are an important source of sediment transport towards the rills. Because rills are also fed with sediment from interrill areas, we might therefore expect that transport capacity will be reached very rapidly, also on very steep sloping areas. To have an idea of the sediment delivery toward the rilling system on an agricultural field, a similar type of transport function was developed for the sheet erosion processes.

This was done using the results of 140 laboratory rainfall simulations. From these 140 laboratory experiments, 133 experiments were carried out in the period from 1973 to 1998 by Pauwels (1973), Gabriels (1974), Verdegem (1979), De Beus (1983), Goossens (1987) and Gabriels et al. (1998). All these experiments were done using sandy, loamy to silty soils. In addition, 7 rainfall experiments were performed on an alluvial clay soil (42 % clay) (Biesemans, 2000). The textural composition of the soils used in all these experiments is given in figure 4.1.

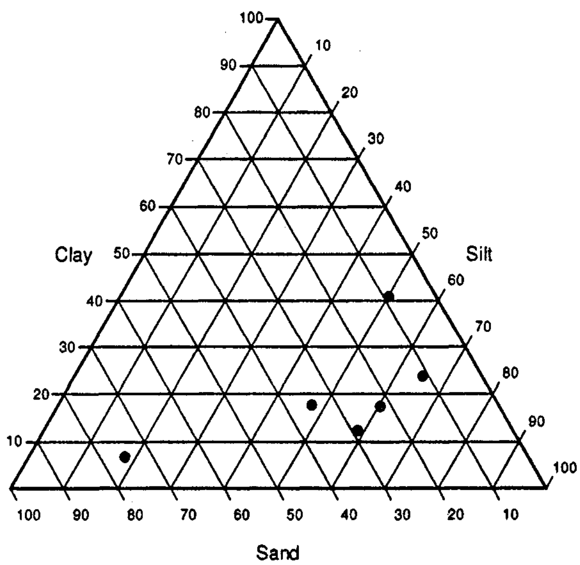

Figure 4.1: *Textural composition of the soil used for the rainfall simulations (Biesemans, 2000).*

All laboratory rainfall experiments were performed on a smoothed surface to prevent possible rilling and to ensure a broad sheet flow during the simulated rain. The intensities of the simulated rain was held constant during the experiments and ranged from 20 to 128 $mm \cdot h^{-1}$. The width of the soil pans was 20 to 30 cm and the length 30 to 90 cm. The slope of the soil pans ranged between 4 and 33 %. The duration of the experiments was between 60 and 120 minutes, and the soil loss was measured at 5 or

10-minute intervals, depending on the intensity of the simulated rain. This resulted in 672 observations of discharge and soil loss.

The measurement of the discharge, Q $(cm^3 \cdot s^{-1})$, is very straightforward: depending on the simulated rainfall intensity, every 5 or 10 minutes the amount of runoff is caught in a graduated cylinder. Because a broad sheet flow is established during the simulations, the width of the flow equals the sample width and the volumetric water flux per unit plane width, q, is directly computable. If the measured unit sediment load, q_s $(g \cdot cm^{-1})$, is log-log plotted against the stream power of the overland flow (figure 4.2), a linear relationship can be identified in the data. This relationship is also a function of the clay content. The higher the clay content, the lower the unit sediment load. On figure 4.2, it can be clearly seen that the unit sediment load is between 1 and 3 log cycles higher for the laboratory rainfall experiments than for the flume experiments of Nearing et al. (1997). This can be explained by the raindrop impact. Because sheet flow is broader and more shallow than rill flow, the momentum of a raindrop impact can act directly upon the soil surface. Consequently, raindrop impact can be considered as the most important soil detachment process in interrill areas. The parameters of the regression power equations, with there corresponding correlation coefficient are also given in figure 4.2. Remark that the exponents of the regression equations are all (except one) around 1.3. The incercept of the regression equations is a measure of the erodibility of the soil. In general, the higher the clay content, the higher the cohesion and the lower the erodibility.

When the erosion processes are observed in the field, the soil loss from an agricultural field towards the drainage system is almost only the result of rill flow. The laboratory rainfall experiments proved that the soil transport from the interrill areas towards the rill system in a field is much higher than the possible transport in a rill (at the same stream power level). Therefore, in the MathCad program (which can be found in the Appendix), only the transport equation for rill flow is used.

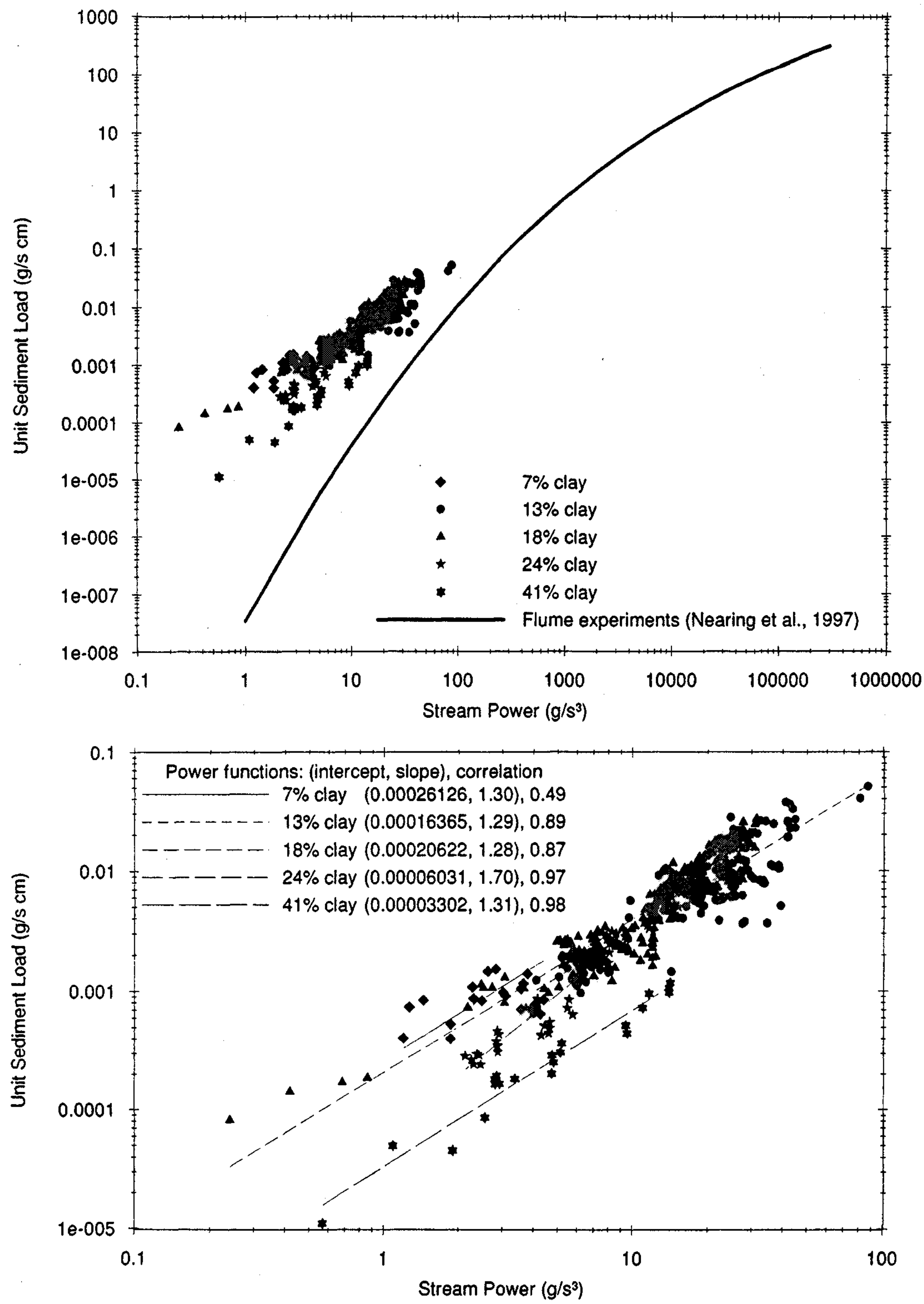

Figure 4.2: *Soil transport function (Biesemans, 2000): stream power as predictor for the unit sediment load. Note that the laboratory flume experiments of Nearing et al. (1997) had a much wider stream power range than the laboratory rainfall experiments.*

Bibliography

Biesemans, J. 2000. Erosion modelling as support for land management in the loess belt of flanders. Ph.D. thesis, Ghent University.

Campbell, G. S. 1985. Soil physics with BASIC, Transport models for soil-plant systems. Elsevier, Amsterdam.

Chow, V. T. 1959. Open-channel hydraulics. McGraw-Hill, New York.

Chow, V. T., D. R. Maidment, and L. W. Mays. 1988. Applied Hydrology. McGraw-Hill, New York.

Clarke, R. T. 1973. Mathematical models in hydrology. Food and Agriculture Organization, Irrigation and Drainage paper 19, Rome.

Courant, R., and K. O. Friedrichs. 1948. Supersonic flow and shock waves. Interscience Publishers, New York.

De Beus, P. 1983. Aggregate distribution in the runoff water as a function of slope length (in Dutch). Master's thesis, University Gent.

de Saint-Venant, B. 1871. Theory of unsteady water flow, with application to river floods and to propagation of tides in river channels. French Academy of Science. 73:148–154,237–240.

Gabriels, D. 1974. Study of the water erosion process by means of rainfall simulation on natural and artificially structured soil samples (in Dutch). Ph.D. thesis, Ghent University.

Gabriels, D., K. Tack, W. M. Cornelis, G. Erpul, D. Norton, and J. Biesemans. 1998. Effect of wind-driven rain on splash detachment and transport of a silt loam soil: a short slope wind-tunnel experiment. In: Proceedings of the International Workshop on technical aspects and use of wind tunnels for wind-erosion control; Combined effect of wind and water on erosion processes, International Centre for Eremology, Ghent University, 87–93.

Goossens, M. 1987. Splash erosion as a factor in the evaluation of soil erodibility (in Dutch). Master's thesis, Ghent University.

Green, W. H., and G. A. Ampt. 1911. Studies on soil physics, Part I: The flow of air and water through soils. J. Agric. Sci. 4(1):1–24.

Ibrahim, H. A., and W. Brutsaert. 1968. Intermittent infiltration into soils with hysteresis. J. Hydraul. Div., ASCE. 94:113–137.

Nearing, M. A., L. D. Norton, D. A. Bulgakov, G. A. Larionov, L. T. West, and K. M. Dontsova. 1997. Hydraulics and erosion in eroding rills. Water Resour. Res. 33(4):865–876.

Pauwels, J. M. 1973. Contribution to the study of water erosion by means of rainfall simulation (in Dutch). Master's thesis, University Gent.

Richards, L. A. 1931. Capillary conduction of liquids through porous mediums. Physics. 1:318–333.

Schmidt, J. 1996. Entwicklung und Anwendung eines physikalisch begründeten Simulations-modells für die Erosion geneigter landwirtschaftlicher Nutzflächen. Berliner Geographische Abhandlungen, Berlin.

Shirazi, M. A., and L. Boersma. 1984. A unifying quantitative analysis of soil texture. Soil. Sci. Soc. Am. J. 48:142–147.

Van Genuchten, M. T. 1980. A closed-form equation for predicting the hydraulic conductivity of unsaturated soils. Soil Sci. Soc. Am. J. 44:892–898.

Verdegem, P. 1979. Effect of slope length on the aggregate size distribution in the runoff water (in Dutch). Master's thesis, Ghent University.

Vereecken, H., J. Maes, J. Feyen, and P. Darius. 1989. Estimating the soil moisture retention characteristic from texture, bulk density, and carbon content. Soil Science. 148(6):389–403.